NANO LETTERS

2006
Vol. 6, No. 12
2690−2695

Design and Tailoring of the Nanotubular Arrayed Architecture of Hydrous RuO_2 for Next Generation Supercapacitors

Chi-Chang Hu,* Kuo-Hsin Chang, Ming-Champ Lin, and Yung-Tai Wu

Laboratory of Electrochemistry and Advanced Materials, Department of Chemical Engineering, National Chung Cheng University, 168 University Road, Min-Hsiung, Chia-Yi 621, Taiwan

Received July 9, 2006; Revised Manuscript Received November 6, 2006

ABSTRACT

By use of the membrane-templated synthesis route, hydrous RuO_2 ($RuO_2 \cdot xH_2O$) nanotubular arrayed electrodes were successfully synthesized by means of the anodic deposition technique. The desired three-dimensional mesoporous architecture of $RuO_2 \cdot xH_2O$ nanotubular arrayed electrodes with annealing in air at 200 °C for 2 h simultaneously maintained the facility of electrolyte penetration, the ease of proton exchange/diffusion, and the metallic conductivity of crystalline RuO_2, exhibiting unexpectedly ultrahigh power characteristics with its frequency "knee" reaching ca. 4.0–7.8 kHz, 20–40 times better than that of RuO_2 single crystalline, arrayed nanorods. The specific power and specific energy of annealed $RuO_2 \cdot xH_2O$ nanotubes measured at 0.8 V and 4 kHz is equal to 4320 kW kg^{-1} and 7.5 W h kg^{-1}, respectively, demonstrating the characteristics of next generation supercapacitors.

Introduction. In development of advanced electrochemical energy storage/conversion devices with both high-power and high-energy densities such as fuel cells, rechargeable batteries, and supercapacitors, an electrode material with three-dimensional (3D), mesoporous, ordered/aperiodic architectures is desirable for the penetration of electrolytes and reactants into the whole electrode matrix.[1−5] However, to obtain the ultrahigh power performance but maintain a high capacity of such devices, e.g., next generation supercapacitors, the electronic resistances in the mesoporous electroactive film and at the interface between electrode materials and current collectors have to be carefully considered. The electronic conductivity of electrode materials is generally promoted by introducing electronic conductors such as carbon black, carbon nanotubes (CNTs), carbon fibers, etc. This action, however, not only reduces the energy density of devices but also adds an extra contact resistance between electronic conductors and active materials without considering the challenges in homogeneous dispersion of active materials, reliable coating techniques, and the contact resistance at the interface between electrode materials and current collectors. The above concerns are especially important in developing the electrode materials of supercapacitors of the next generation whose power characteristics are designed to achieve as high as ∼20 kW kg^{-1} or higher (based on the mass of device). Therefore, an electroactive material with metallic conductivity and a desirable, 3D mesoporous structure not only reduces the diffusion resistance of electrolytes but also enhances the facility of ion transportation and maintains the very smooth electron pathways in the very rapid charge/discharge reactions. Accordingly, achieving the ultrahigh power and retaining a high capacity for next generation supercapacitors become possible.[4]

Due to the unique characteristics, such as metallic conductivity,[6] high chemical and thermal stability,[7,8] catalytic activities,[9−12] electrochemical redox properties,[4,9,13] and field-emitting behavior,[14] RuO_2 in both crystalline and amorphous forms is of both academic and practical importance. For example, in electronic applications, RuO_2 films showed great promise in integrated circuit development,[15] thick or thin film resistors,[16,17] ferroelectric films,[18] and a buffer layer for the high-temperature superconducting thin film.[19] In catalysis, RuO_2 is the active component in dimensionally stable anodes for chlorine generation in the chlor-alkali industry,[9] oxygen or hydrogen evolution in water electrolysis,[10] CO_2 reduction in photocatalysis,[11] and CO oxidation in sensors.[12] In energy storage/conversion devices, ruthenium hydroxide is an essential element removing the CO-like poisoning in the Pt−Ru anodes of the direct methanol fuel cells.[20] In addition, $RuO_2 \cdot xH_2O$ is the most promising electrode material for electrochemical supercapacitors due to its intrinsic reversibility of surface redox couples[21] and the ultrahigh pseudocapacitance.[13,22] However, such high specific capacitance cannot be maintained under high power operation,[23] which is commonly found for most electroactive materials. More-

* Corresponding author. E-mail: chmhcc@ccu.edu.tw.

10.1021/nl061576a CCC: $33.50
Published on Web 11/18/2006

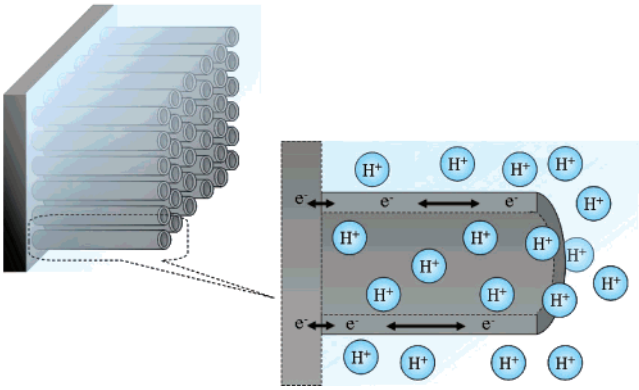

Figure 1. An ideal design of the electrode material for next generation supercapacitors, $RuO_2 \cdot xH_2O$ nanotubular arrayed electrode. The mesoporous architecture, hydrous nature, and metallic conductivity provide the proton and electron "superhighways" for the extremely rapid charge/discharge processes.

over, the low specific capacitance of thick, crystalline RuO_2 films has been attributed to the presence of inactive, bulk crystalline RuO_2 layer and the significant length of proton diffusion.[9,21,24,25] On the basis of the above viewpoints, how to simultaneously construct the smooth pathways of both electrons and electrolytes for the extremely rapid charge/discharge processes of the supercapacitors of the next generation, a typical ultrahigh power device, is an unavoidable issue.[4,26]

Background. We design a desired schematic structure (shown in Figure 1), i.e., a $RuO_2 \cdot xH_2O$ nanotubular arrayed electrode, for such an application. In this scheme, the crystalline $RuO_2 \cdot xH_2O$ nanotubes (NTs) (and the $RuO_2 \cdot xH_2O$ underlayer) with metallic conductivity will provide the electron "superhighways" for charge storage and delivery. The arrayed, porous architecture of $RuO_2 \cdot xH_2O$ NTs substantially reduces the resistance of electrolyte penetration/diffusion. Moreover, the hydrous nature of $RuO_2 \cdot xH_2O$ promotes the rate of proton exchange (very different from the anodic aluminum oxide assisted, anhydrous RuO_2 nanotubes prepared by means of thermal decomposition[27]) since the superficial redox transitions of RuO_2 involve the proton and electron double injecting/expelling process, expressed as follows[21,28]

$$RuO_a(OH)_b + \delta H^+ + \delta e^- \leftrightarrow RuO_{a-\delta}(OH)_{b+\delta}$$

Accordingly, this desired 3D mesoporous architecture will definitely reduce the equivalent series resistance (ESR, a lumping parameter considering the whole charge/discharge impedance) by simultaneously maintaining the facile electrolyte penetration, fast proton exchange, and the metallic conductivity.

In general, materials with nanostructures in high aspect ratios, such as nanowires and NTs, have been widely prepared by means of membrane-templated synthesis routes, including electroless deposition, sol−gel synthesis, chemical vapor deposition, layer-by-layer method, and electrochemical deposition,[29,30] etc. Among these methods, anodic deposition of $RuO_2 \cdot xH_2O$ NTs is employed due to its simplicity, one-step process, reliability, low cost, versatility, and the hydrous nature of oxides, especially due to the fact that electrochemical deposition is a powerful method for the large-scale production. Although anodic deposition has been widely used to prepare various transition metal oxides, to the best of our knowledge, this work is the first report successfully demonstrating the anodic deposition of $RuO_2 \cdot xH_2O$ from its chloride precursor. Moreover, nanowires are generally preferred to form through filling of the pores within templates by means of electrochemical deposition because most templates are insulators (e.g., anodic aluminum oxide (AAO) and track-etched polymer membranes) although the formation of H_2 bubbles within the templates was proposed to depress the filling of nanopores, resulting in the presence of tubular structure during the cathodic deposition of metals.[31] The above two challenges have been overcome, and ideal capacitive performances (e.g., ultrahigh specific capacitance of ca. 1300 F g^{-1}, excellent charge/discharge behavior at 1000 mV s^{-1}, and high-frequency (4.0∼7.8 kHz) capacitive responses) of $RuO_2 \cdot xH_2O$ NTs plated by anodic deposition have been obtained in this work.

Textural Characterization of $RuO_2 \cdot xH_2O$ Nanotubular Arrayed Architecture Prepared by Anodic Deposition. Hydrous ruthenium oxides were successfully deposited onto Ti substrates from aqueous ruthenium chloride solutions by using the potentiodynamic (CV) deposition technique in our laboratory,[32] while it is not easy to directly deposit $RuO_2 \cdot xH_2O$ onto carbon (due to oxidative attack)[33] or Ti (due to passivation of substrates) under the anodic, potentiostatic/galvonostatic plating modes. The above issues can be effectively overcome by using a conductive binder, consisting of 95 wt % $RuO_2 \cdot xH_2O$ nanocrystallites prepared by a hydrothermal synthesis method[4] and 5 wt % polyvinylidene difluoride (PVdF), between the AAO membrane and substrates. The maximum deposition rate can be promoted by adding excess acetate ions as the complex agent into the $RuCl_3 \cdot xH_2O$ solution. Parts A and B of Figure 2 show the scanning electron microscopic (SEM) top images of $RuO_2 \cdot xH_2O$ NTs prepared by anodic deposition at 1.0 V for 20 min after removing the AAO template. The homogeneous opening reveals the success in the formation of a nanotubular arrayed structure. The opening surface of these NTs is very rough, which implies the adherent stacking of $RuO_2 \cdot xH_2O$ particulates from bottom of pores within the AAO membrane, resulting in the formation of these NTs. Due to the metallic conductivity, the length of $RuO_2 \cdot xH_2O$ NTs can be controlled by monitoring the variation in the deposition current density (Figure 2C). During the deposition, a gradual increase in the current density is observed at the onset of overfilling due to the extension of effective surface area, which is clearly found from the onset-overfilled morphology (Figure 2D).

The nanotubular structure is more clearly found in the TEM images of $RuO_2 \cdot xH_2O$ NTs annealed at 200 °C for 2 h (Figure 3A). The very uniform wall thickness of these $RuO_2 \cdot xH_2O$ NTs is ∼40 ± 5 nm which is very desirable for the supercapacitor application (see below), although some particulates adherent to the wall are visible. The outer

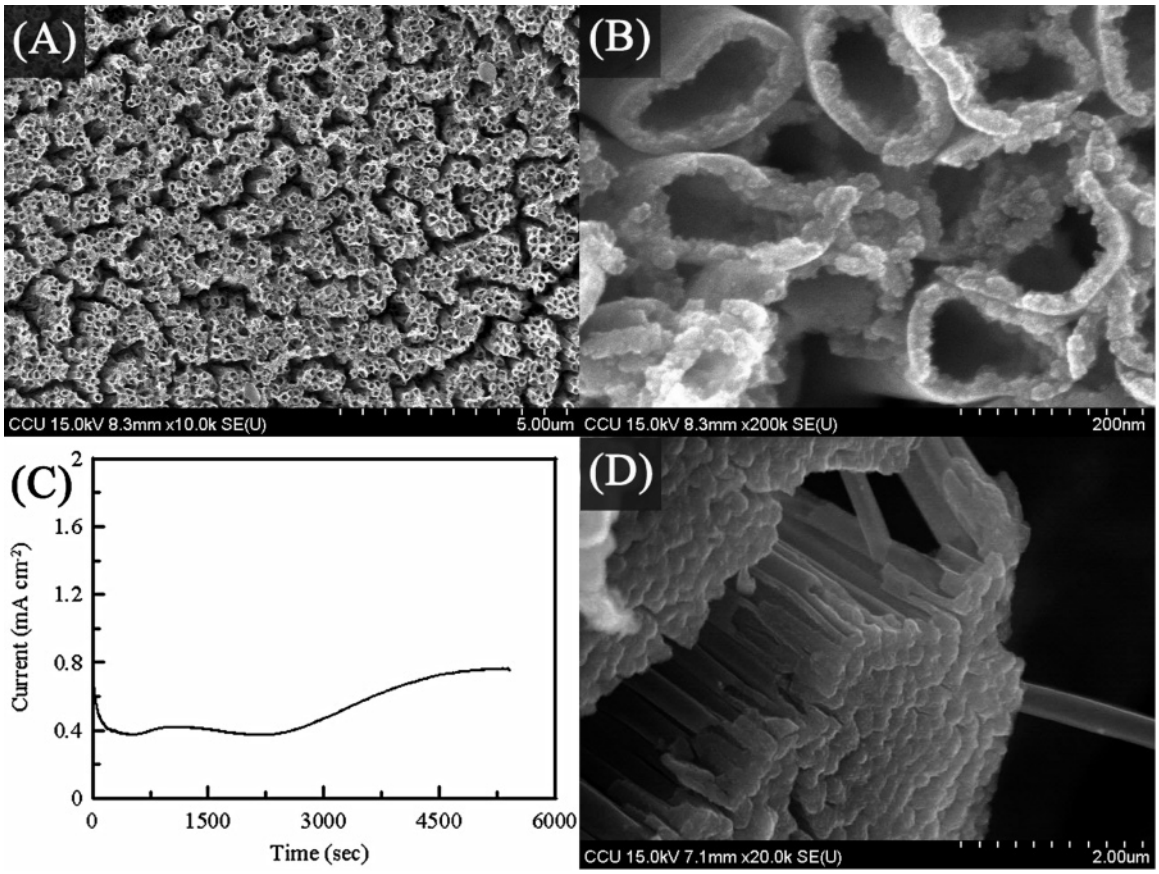

Figure 2. (A, B) SEM top images of an $RuO_2 \cdot xH_2O$ NTs arrayed electrode. (C) The $i-t$ curve of anodic deposition measured at 1.0 V from a 10 mM $RuCl_3 \cdot xH_2O$ + 0.1 M CH_3COONa solution. (D) A SEM image showing the onset−overfilled morphology of a $RuO_2 \cdot xH_2O$ NT arrayed electrode. All NTs were deposited at 1.0 V from a 10 mM $RuCl_3 \cdot xH_2O$ + 0.1 M CH_3COONa solution.

diameter of NTs is about 200 ± 20 nm corresponding to the diameter of AAO templates used, supporting the idea that $RuO_2 \cdot xH_2O$ grains are adherently stacked to form the tubular structure. The selected area electron diffraction pattern reveals the polycrystalline structure in the rutile form for the annealed $RuO_2 \cdot xH_2O$ NTs (see inset of Figure 3A). The interplanar spacing of crystalline grain was calculated to be ~0.25 nm, corresponding to the same orientation of atomic plane (101) in the rutile form of RuO_2 (see Figure 3B). On the basis of the thermogravimetric analysis results (see Supporting Information), the as-deposited and annealed oxides correspond to $RuO_2 \cdot 1.8H_2O$ and $RuO_2 \cdot 0.78H_2O$, respectively.

Electrochemical Characterization of $RuO_2 \cdot xH_2O$ Nanotubular Arrayed Electrodes. The ordered, 3D, porous architecture is favorable for the penetration of electrolytes into the whole oxide matrix, and the hydrous structure shortens the proton diffusion distance. Therefore, high specific capacitance of 740 F g^{-1} for the as-deposited $RuO_2 \cdot xH_2O$ NTs is obtained, where the specific capacitance of $RuO_2 \cdot xH_2O$ reported in this work is based on the total mass of $RuO_2 \cdot xH_2O$ NTs and $RuO_2 \cdot xH_2O$ + PVdF binder on the electrodes. In order to simultaneously construct the "superhighways" of protons and electrons for the redox transitions of oxyruthenium species between various oxidation states, annealing is a necessary step to promote the capacitive performances of $RuO_2 \cdot xH_2O$.[28] In addition, the stability of $RuO_2 \cdot xH_2O$ has been found to further improve by the formation and growth of RuO_2 crystallites.[4,21−23,28] The total specific capacitance of $RuO_2 \cdot xH_2O$ is promoted from 740 to 1300 F g^{-1} when these NTs are annealed in air at 200 °C for 2 h. This ultrahigh value of specific capacitance in never found for a pure, bulk, nanostructured $RuO_2 \cdot xH_2O$ electrode although the theoretical value of $RuO_2 \cdot xH_2O$ nanoparticulates was estimated to range from ca. 1300 to 2200 F g^{-1} and the maximum utilization of $RuO_2 \cdot xH_2O$ within carbon−RuO_2 composites was found to reach as high as 1580 F g^{-1} in our previous work.[22,34] The above ultrahigh specific capacitance, indicative of a full utilization of $RuO_2 \cdot xH_2O$, is reasonably attributed to the thin (~40 nm) but uniform walls of $RuO_2 \cdot xH_2O$ NTs, resulting in the absence of a rigid, crystalline RuO_2 layer.[24,25]

The rectangle-like shape of all $i-E$ curves measured at various scan rates in 1.0 M H_2SO_4 (Figure 4A) for the annealed $RuO_2 \cdot xH_2O$ NTs reveals the perfect electrochemical reversibility of the Faradaic redox transitions on these oxide NTs. This ideal pseudocapacitive behavior at very high scan rates cannot be found for most $RuO_2 \cdot xH_2O$, with the exception of $RuO_2 \cdot xH_2O$ nanocrystallites prepared by a hydrothermal synthesis technique[4,35] or anhydrous, single-crystalline RuO_2 nanorods formed by a chemical vapor deposition (CVD) process.[36] For both cases, unfortunately, the specific capacitance of $RuO_2 \cdot xH_2O$ is much lower than that of $RuO_2 \cdot xH_2O$ NTs. Actually, the poor capacitive

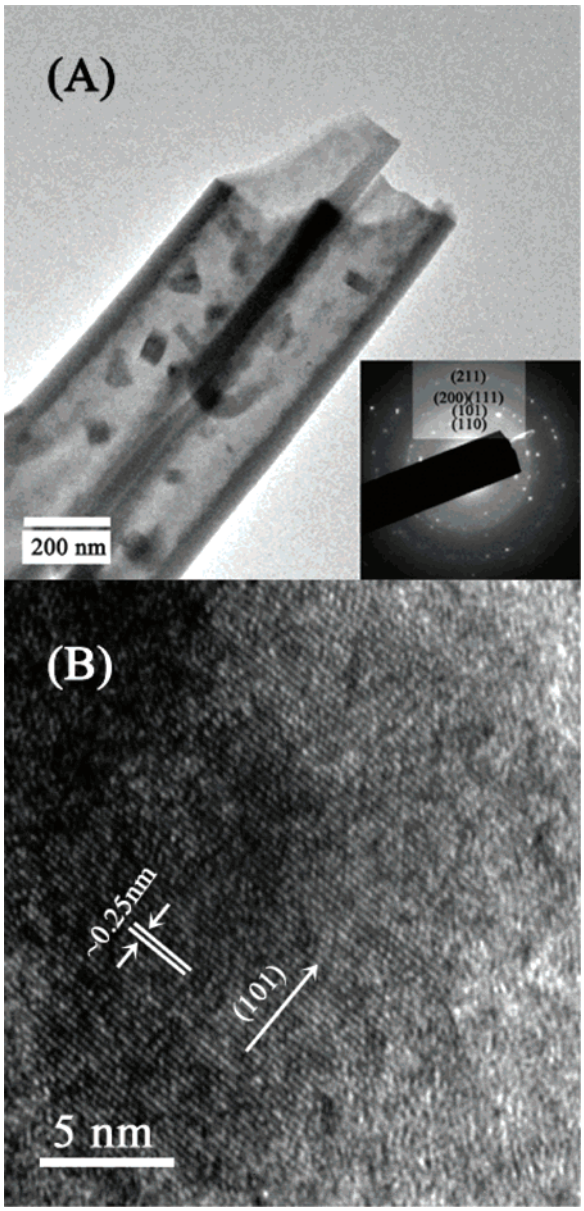

Figure 3. (A) The bright-field and (B) high-resolution TEM images of $RuO_2 \cdot xH_2O$ NTs annealed in air at 200 °C for 2 h. The inset of electron diffraction pattern shows typical diffraction rings of RuO_2 polycrystals in the rutile form.

performance at very high scan rates is a common issue for all electroactive materials in the application of supercapacitors, usually due to the significant barrier for the penetration and diffusion of electrolytes into a relatively thick film and/or the relatively poor electronic conductivity of active materials. Moreover, the loss in specific capacitance upon increasing the scan rate is very obvious (e.g., see ref 37, 59% loss as the scan rate varied from 2 to 100 mV s^{-1} for the case of 0.25 mg cm^{-2}), which becomes more serious with increasing the loading of active materials (reaching 85% is possible). For thick, crystalline RuO_2 layers, the dependence of specific capacitance on the scan rate of CV has been schemed as a three-layer model consisting of a bulk layer of rigid, crystalline RuO_2, an inner layer of partially hydrated RuO_2 being less proton accessible, and an outer, proton-accessible layer of hyperextended oxyruthenium species.[24] Therefore, ultrathin electroactive films or a tiny amount of active particles (e.g., for MnO_2 with mass ≈5 μg)[38] dispersed onto an electrode generally show extremely high specific capacitance while their very low capacity is practically unacceptable. The above drawback is relatively minor for annealed $RuO_2 \cdot xH_2O$ NTs (Figure 4B for the electrode with 0.19 mg cm^{-2}, only 40% loss as the scan rate varied from 10 to 1000 mV s^{-1}). The above excellent performance is reasonably attributed to the novel nanotubular arrayed structure of $RuO_2 \cdot xH_2O$, which not only reduces the diffusion distance of protons (maximal length ≈20 nm) but also increases the facility of ion transportation during the rapid charge/discharge reactions. In addition, the metallic conductivity of annealed, crystalline $RuO_2 \cdot xH_2O$ NTs provides the "superhighways" for electron hopping.

The perfect performances of annealed $RuO_2 \cdot xH_2O$ NTs in supercapacitors are further demonstrated by the unexpectedly high-frequency capacitive responses (see Supporting Information, the "knee" frequency reaches ca. 4.0−7.8 kHz in Figure S3(A) and a phase angle at −45° reaches ca. 5−8 Hz from Figure S3(C)) measured in a three-compartment cell. The former characteristic, about 20−40 times better than that of anhydrous, single-crystalline, metal-conductive RuO_2 nanorods formed by a CVD process,[36] indicates the extremely low ESR of annealed $RuO_2 \cdot xH_2O$ NTs, revealing their ultrahigh power nature for supercapacitors of the next generation. The latter property is somewhat better than that of $RuO_2 \cdot 0.5H_2O$ and ruthenium acid nanosheets (ca. 2−5 Hz at −45°), which have been demonstrated to exhibit ideal capacitive performances.[13,23,26] Moreover, the total specific capacitance measured at 4 kHz and 100 Hz (corresponding to a scan rate of 160 and 4 V s^{-1}, respectively) at 0.8 V is as high as 54 and 550 F g^{-1} (Figure 4D), respectively. The specific power and specific energy of annealed $RuO_2 \cdot xH_2O$ NTs measured at 0.8 V and 100 Hz is equal to 1100 kW kg^{-1} and 76.4 W h kg^{-1}, respectively, which corresponds to 4320 kW kg^{-1} and 7.5 W h kg^{-1}, respectively, when the applied frequency is equal to 4 kHz. The above achievements reveal the perfect performances of annealed $RuO_2 \cdot xH_2O$ NTs for supercapacitors of the next generation.

Conclusions. We successfully designed and tailored an advanced electrode material with a 3D, arrayed, nanotubular architecture—annealed $RuO_2 \cdot xH_2O$ NTs which achieve the performances (ultrahigh-power characteristics and high capacity) required for next generation supercapacitors by using a very simple, one-step, reliable, cost-effective, anodic deposition technique. This unique structure not only reduces the diffusion resistance of electrolytes but also enhances the facility of ion transportation and maintains the very smooth electron pathways for the extremely rapid charge/discharge reactions. The specific power and specific energy of $RuO_2 \cdot xH_2O$ nanotubular arrayed electrodes (with annealing in air at 200 °C for 2 h) measured at 0.8 V and 4 kHz is equal to 4320 kW kg^{-1} and 7.5 W h kg^{-1}, respectively, achieving the perfect performance for next generation supercapacitors, which is never found in the literature. On the other hand, from parts A and B of Figure 2, the number density of $RuO_2 \cdot xH_2O$ nanotubes in the array layer is not

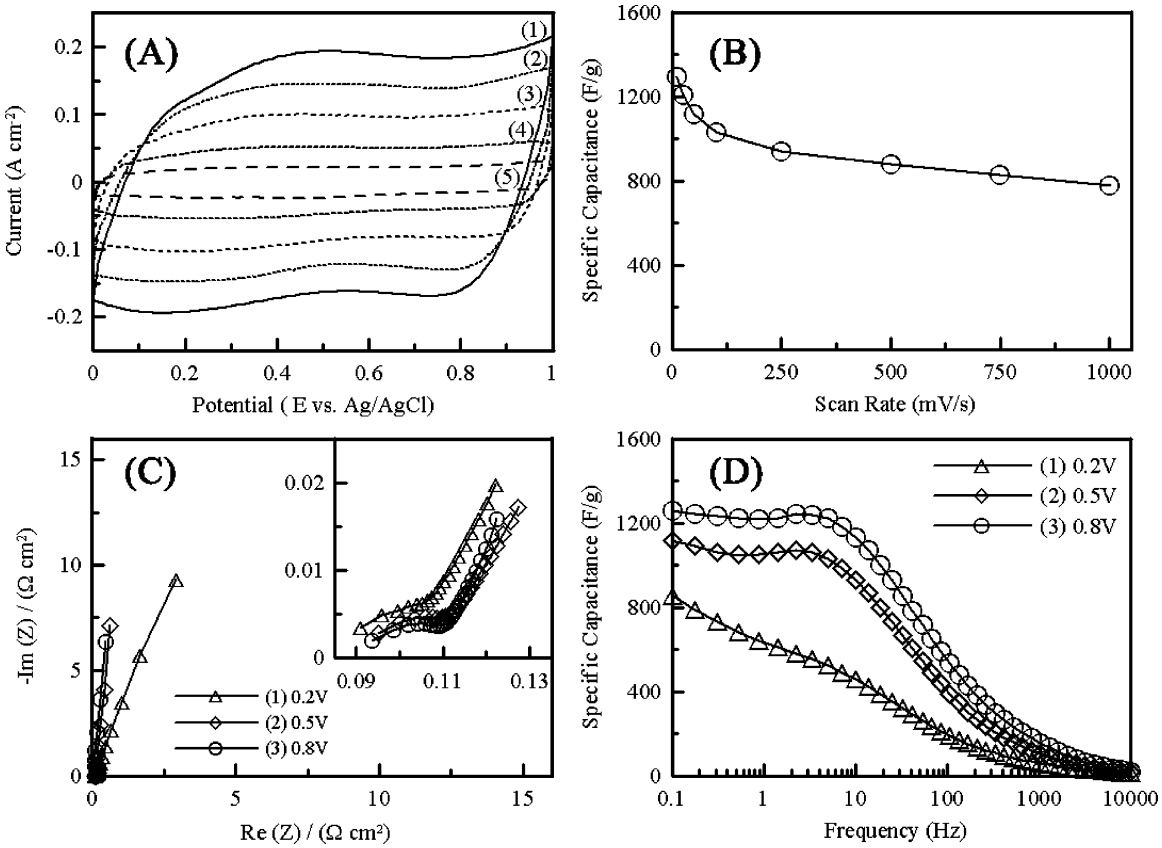

Figure 4. (A) Cyclic voltammograms measured at (1) 1000, (2) 750, (3) 500, (4) 250, and (5) 100 mV s^{-1}, and (B) dependence of the capacitance loss on the scan rate of CV from 10 to 1000 mV s^{-1} for an annealed $RuO_2 \cdot xH_2O$ NT arrayed electrode (0.19 ± 0.01 mg cm^{-2}). (C) Electrochemical impedance spectra measured at various potentials with potential amplitude of 10 mV. (D) Frequency dependence of specific capacitance for an annealed $RuO_2 \cdot xH_2O$ NT arrayed electrode (0.21 ± 0.01 mg cm^{-2}). The electrolyte for electrochemical analyses is 1.0 M H_2SO_4.

high, which usually results in a low volumetric specific capacitance (in F cm^{-3}). The number density of $RuO_2 \cdot xH_2O$ nanotubes, unfortunately, depends on the pore density of AAO templates, which is believed to greatly improve by controlling the pore size and density of templates since the high volumetric specific capacitance is as important as the high gravimetric specific capacitance (in F g^{-1}) for most applications.

Methods. *Deposition of $RuO_2 \cdot xH_2O$ Nanotubular Array and Electrode Preparation.* Hydrous ruthenium oxide ($RuO_2 \cdot xH_2O$) NTs were electrodeposited onto AAO-coated graphite (10 × 10 × 3 mm) or Ti substrates (10 × 10 × 0.5 mm). The pretreatments corresponding to graphite and Ti substrates completely followed our previous work.[22,32] For comparison purposes, all data shown in this work are based on the graphite substrate. Following the pretreatments of substrates, a mixture consisting of 95 wt % $RuO_2 \cdot xH_2O$ nanocrystallites prepared by a hydrothermal synthesis method and 5 wt % polyvinylidene difluoride (PVdF) was used as the binder between the AAO membrane and substrates. These electrodes were carefully coated with a thick film of epoxy resin with an exposed surface area of 1 cm^2, and then $RuO_2 \cdot xH_2O$ NTs were electroplated from $RuCl_3$ + CH_3COONa aqueous solutions (a typical solution consisting of 10 mM $RuCl_3 \cdot xH_2O$ (Alfa Aesar) + 0.1 M NaAcO (Merck)) at 1.0 V for 10−30 min. After deposition, AAO and epoxy resin were removed and $RuO_2 \cdot xH_2O$ NTs were repeatedly degreased with pure water and finally dried at room temperature under a reduced pressure. Some of these electrodes were subjected to annealing at 200 °C for 2 h to further enhance the capacitive performances of $RuO_2 \cdot xH_2O$ NTs. The specific capacitance reported in this work is based on the total mass of $RuO_2 \cdot xH_2O$ NTs and $RuO_2 \cdot xH_2O$+PVdF binder on the electrodes. The total oxide loading (∼0.12−0.3 (±0.01) mg cm^{-2}) is the weight difference of an electrode without epoxy resin and AAO before and after the application of oxide deposition, obtained with a microbalance with an accuracy of 10 μg (Sartorius BP 211D). All electrodes have an exposed surface area of 1 cm^2 for electrochemical characterization.

Characterization. The surface morphology of $RuO_2 \cdot xH_2O$ NTs was observed through a field emission scanning electron microscope (FE-SEM, Hitachi S-4800). The nanostructures of oxides were examined by means of a field emission gun transmission electron microscope (FE-TEM, Philips Tecnai G2 F20). Electrochemical characteristics of $RuO_2 \cdot xH_2O$ NTs were examined by means of an electrochemical analyzer system, CHI 633A (CH Instruments, USA), in a three-compartment cell. The impedance spectrum analyzer, IM6 (ZAHNER), with Thales software was employed to measure and analyze the EIS data. The potential amplitude of ac is equal to 10 mV, meanwhile its frequency region is from 0.1 to 100 kHz. An Ag/AgCl electrode (Argenthal, 3 M KCl,

0.207 V vs SHE at 25 °C) was used as the reference, and a piece of platinum gauze was employed as the counter electrode. A Luggin capillary was used to minimize errors due to *iR* drop in the electrolytes. All solutions used in this work were prepared with 18 MΩ cm water produced by a reagent water system (Milli-Q SP, Japan).

Acknowledgment. The financial support of this work, by the National Science Council of ROC, under Contract No. NSC 94-2214-E-194-003, is gratefully acknowledged. The authors deeply appreciate Professor Wen-Tsang Wu at Southern Taiwan University of Technology and Ph.D. Candidate Mr. Kuo-Min Lin at National Chung Cheng University for the help with HR-TEM and SEM, respectively.

Supporting Information Available: Graphs of thermogravimetric analysis (TGA), differential thermal analysis, and detailed impedance analyses of the as-deposited and annealed $RuO_2 \cdot xH_2O$ NTs and micrographs showing control of the length of $RuO_2 \cdot xH_2O$ NTs. This material is available free of charge via the Internet at http://pubs.acs.org.

References

(1) Che, G.; Lakshmi, B. B.; Fisher, E. R.; Martin, C. R. *Nature* **1998**, *393*, 346.
(2) (a) Long, J. W.; Dunn, B.; Rolison, D. R.; White, H. S. *Chem. Rev.* **2004**, *104*, 4463. (b) Long, J. W.; Rhodes, C. P.; Young, A. L.; Rolison, D. R. *Nano Lett.* **2003**, *3*, 1155. (c) Anderson, M. L.; Stroud, R. M.; Rolison, D. R. *Nano Lett.* **2002**, *2*, 235.
(3) Sides, C. R.; Martin, C. R. *Adv. Mater.* **2005**, *17*, 125.
(4) Chang, K. H.; Hu, C. C. *Appl. Phys. Lett.* **2006**, *88*, 193102.
(5) Niu, C.; Sichel, E. K.; Hoch, R.; Moy, D.; Tennent, H. *Appl. Phys. Lett.* **1997**, *70*, 1480.
(6) Schafer, H.; Schneidereit, G.; Gerhardt, W. *Z. Anorg. Allg. Chem.* **1962**, *319*, 327.
(7) Campbell, P. F.; Ortner, M. H.; Anderson, C. *J. Anal. Chem.* **1961**, *33*, 58.
(8) Vadimsky, R. G.; Frankenthal, R. P.; Thompson, D. E. *J. Electrochem. Soc.* **1979**, *126*, 2017.
(9) Trasatti, S. *Electrochim. Acta* **1991**, *36*, 225.
(10) Kotz, E. R.; Stucki, S. *J. Appl. Electrochem.* **1987**, *17*, 1190.
(11) Popic, J. P.; Avramov-Ivic, M. L.; Vukovic, N. B. *J. Electroanal. Chem.* **1997**, *421*, 105.
(12) Over, H.; Kim, Y. D.; Seitsonen, A. P.; Wendt, S.; Lundgren, E.; Schmid, M.; Varga, P.; Morgante, A.; Ertl, G. *Science* **2000**, *287*, 1474.
(13) (a) Zheng, J. P.; Jow, T. R. *J. Electrochem. Soc.* **1995**, *142*, L6. (b) Zheng, J. P.; Cygan, P. J.; Jow, T. R. *J. Electrochem. Soc.* **1995**, *142*, 2699.
(14) Cheng, C. L.; Chen, Y. F.; Chen, R. S.; Huang, Y. S. *Appl. Phys. Lett.* **2005**, *86*, 103104.
(15) Krusin-Elbaum, L.; Wittmer, M. *J. Electrochem. Soc.* **1988**, *135*, 2610.
(16) Khanna, P. K.; Bhatnagar, S. K.; Sisodia, M. L. *J. Phys. D* **1988**, *21*, 1766.
(17) Jia, Q. X.; Shi, Z. Q.; Jiao, K. L.; Anderson, W. A. *Thin Solid Films* **1991**, *196*, 29.
(18) Vijay, D. P.; Desu, S. B. *J. Electrochem. Soc.* **1993**, *140*, 2640.
(19) Jia, Q. X.; Anderson, W. A. *Appl. Phys. Lett.* **1990**, *57*, 304.
(20) Rolison, D. R.; Hagans, P. L.; Swider, K. E.; Long, J. W. *Langmuir* **1999**, *15*, 774.
(21) Conway, B. E. *Electrochemical Supercapacitors*; Kluwer Academic/Plenum: New York, 1999.
(22) Hu, C. C.; Chen, W. C.; Chang, K. H. *J. Electrochem. Soc.* **2004**, *151*, A281.
(23) Sugimoto, W.; Iwata, H.; Yokoshima, K.; Murakami, Y.; Takasu, Y. *J. Phys. Chem. B* **2005**, *109*, 7330.
(24) Liu, T.; Pell, W. G.; Conway, B. E. *Electrochim. Acta* **1997**, *42*, 3541.
(25) Ardizzone, S.; Fregonara, G.; Trasatti, S. *Electrochim. Acta* **1990**, *35*, 263.
(26) Sugimoto, W.; Iwata, H.; Yasunaga, Y.; Murakami, Y.; Takasu, Y. *Angew. Chem. Int. Ed.* **2003**, *42*, 4092.
(27) Tan, H.; Ye, E.; Fan, W. Y. *Adv. Mater.* **2006**, *18*, 619.
(28) Dmowski, W.; Egami, T.; Swider-Lyons, K. E.; Love, C. T.; Rolison, D. R. *J. Phys. Chem. B* **2002**, *106*, 12677.
(29) Hulteen, J. C.; Martin, C. R. *J. Mater. Chem.* **1997**, *7*, 1075.
(30) Hurst, S. J.; Payne, E. K.; Qin, L.; Mirkin, C. A. *Angew. Chem., Int. Ed.* **2006**, *45*, 2672.
(31) Fukunaka, Y.; Motoyama, M.; Konishi, Y.; Ishii, R. *Electrochem. Solid-State Lett.* **2006**, *9*, C62.
(32) Hu, C. C.; Huang, Y. H. *J. Electrochem. Soc.* **1999**, *146*, 2465.
(33) Wang, C. C.; Hu, C. C. *Carbon* **2005**, *43*, 1926.
(34) Hu, C. C.; Chen, W. C. *Electrochim. Acta* **2004**, *49*, 3469.
(35) Chang, K. H.; Hu, C. C. *Electrochem. Solid-State Lett.* **2004**, *7*, A466.
(36) Ke, Y. F.; Tsai, D. S.; Huang, Y. S. *J. Mater. Chem.* **2005**, *15*, 2122.
(37) Choi, D.; Blomgren, G. E.; Kumta, P. N. *Adv. Mater.* **2006**, *18*, 1178.
(38) Toupin, M.; Brousse, T.; Belanger, D. *Mater. Chem.* **2004**, *16*, 3184.

NL061576A